



Insights into the origin of carbonaceous chondrite organics from their triple oxygen isotope composition

Romain Tartèse^{a,1}, Marc Chaussidon^b, Andrey Gurenko^c, Frédéric Delarue^d, and François Robert^e

^aSchool of Earth and Environmental Sciences, The University of Manchester, Manchester M13 9PL, United Kingdom; ^bInstitut de Physique du Globe de Paris, Université Sorbonne-Paris-Cité, Université Paris Diderot, CNRS UMR 7154, F-75238 Paris, France; ^cCentre de Recherches Pétrographiques et Géochimiques, UMR 7358, Université de Lorraine, F-54501 Vandoeuvre-lès-Nancy, France; ^dSorbonne Université, Université Pierre-et-Marie-Curie, CNRS, École Pratique des Hautes Etudes, Paris Sciences et Lettres, UMR 7619 Milieux Environnementaux, Transferts et Interactions dans les Hydrosystèmes et les Sols, F-75005 Paris, France; and ^eInstitut de Minéralogie, de Physique des Matériaux et de Cosmochimie, Muséum National d'Histoire Naturelle, Sorbonne Universités, CNRS, Université Pierre-et-Marie-Curie, and Institut de Recherche pour le Développement, F-75005 Paris, France

Edited by Mark H. Thiemens, University of California, San Diego, La Jolla, CA, and approved July 12, 2018 (received for review May 10, 2018)

Dust grains of organic matter were the main reservoir of C and N in the forming Solar System and are thus considered to be an essential ingredient for the emergence of life. However, the physical environment and the chemical mechanisms at the origin of these organic grains are still highly debated. In this study, we report high-precision triple oxygen isotope composition for insoluble organic matter isolated from three emblematic carbonaceous chondrites, Orgueil, Murchison, and Cold Bokkeveld. These results suggest that the O isotope composition of carbonaceous chondrite insoluble organic matter falls on a slope 1 correlation line in the triple oxygen isotope diagram. The lack of detectable mass-dependent O isotopic fractionation, indicated by the slope 1 line, suggests that the bulk of carbonaceous chondrite organics did not form on asteroidal parent bodies during low-temperature hydrothermal events. On the other hand, these O isotope data, together with the H and N isotope characteristics of insoluble organic matter, may indicate that parent bodies of different carbonaceous chondrite types largely accreted organics formed locally in the protosolar nebula, possibly by photochemical dissociation of C-rich precursors.

carbonaceous chondrites | organic matter | oxygen isotopes | protosolar nebula | secondary ion mass spectrometry

Type 1–2 carbonaceous chondrites (CCs) contain several weight percent (wt%) carbon that mostly occurs as small patches of organic matter (OM) dispersed in the fine-grained matrix (1). Because this OM possibly played a key role in the development of life on the early Earth, its molecular structure and its chemical and isotopic compositions have been extensively investigated (see ref. 2 and references therein for a recent review). Despite this profusion of structural, chemical, and isotopic information, the question of whether CC OM formed in the cold interstellar medium (e.g., refs. 3–5), formed in the protosolar nebula (PSN) (e.g., refs. 6–9), or is a product of organic synthesis during hydrothermalism on CC parent bodies (e.g., ref. 10) remains highly debated, notably because the extent of chemical and isotopic alteration of OM during secondary processes on CC parent bodies is unclear (11–15).

Oxygen is the third most abundant element in the Solar System and has three stable isotopes, ¹⁶O, ¹⁷O, and ¹⁸O. Because different fractionation laws govern interplanetary and intra-planetary processes (e.g., ref. 16), the oxygen three-isotope system can provide information that cannot be accessed using other two-isotope systems of light elements such as H, C, and N. In planetary bodies, variations of the ¹⁷O/¹⁶O and ¹⁸O/¹⁶O ratios almost always obey the mass-dependent relationship $\delta^{17}\text{O} \sim 0.52 \times \delta^{18}\text{O}$, while oxygen isotope abundance variations between Solar System gas and solids are primarily governed by the mass-independent relationship $\delta^{17}\text{O} \sim 1.0 \times \delta^{18}\text{O}$ (15). [This δ -notation represents deviations in parts per 1,000 (‰) of the ^{17,18}O/¹⁶O ratios relative to those of the standard mean ocean water (SMOW), according to the equation $\delta^{17,18}\text{O} = [(\text{^{17,18}O/^{16}O})_{\text{sample}} / (\text{^{17,18}O/^{16}O})_{\text{SMOW}} - 1] \times 1,000$.] Much of our understanding of how our Solar System formed and evolved is thus based on O isotope

studies of meteoritic materials (e.g., refs. 16 and 17), and this should apply to CC OM since it contains ~10–25 wt% O (11, 12).

However, determining the O isotope composition of OM is challenging since it tends to be intimately mixed with O-rich silicates and oxides at nanoscale to microscale in carbonaceous chondrites (e.g., ref. 18). Acid maceration used to isolate the insoluble OM (IOM) fraction from whole-rock samples removes most of the silicates but is less effective at dissolving sulfides and some refractory O-bearing oxides such as chromite, spinel, hironite, or corundum. Bulk pyrolysis O isotope analysis of IOM is thus susceptible to contamination by residual mineral inclusions. To constrain the triple O isotope composition of CC IOM, we integrate here high spatial resolution secondary ion mass spectrometry (SIMS) data obtained using NanoSIMS with high-precision ^{17,18}O/¹⁶O isotope ratios obtained using large geometry multicollector IMS 1270/80 ion probes (referred to as L-SIMS in the following). For each L-SIMS O isotope analysis, measurement of ²⁸Si, ³²S, and ⁵⁶Fe/¹⁶O intensities allowed a first-order filtering of data for which the O signals were largely affected by contamination by residual silicate and/or oxide phases (see *Materials and Methods* for details). The results presented here thus provide high-precision triple O isotope estimates for IOM residues isolated from two emblematic CC falls, the Ivuna-type (CI) Orgueil meteorite and the Mighei-type (CM) Murchison meteorite.

Significance

Refractory organic matter found in volatile-rich asteroidal materials essentially comprise the elements C, H, O, N, and S, which are thought to be important building blocks for life. Characterizing the origin(s) of these organics thus constitutes a key step to constrain the origin of life on Earth and appraise the habitability potential of other worlds. However, how and where these organics formed are still highly debated. In this study, we have determined the oxygen isotope composition of refractory organics from two families of carbonaceous chondrites. These data suggest that these organics formed in the nascent Solar System, possibly through chemical reactions occurring in the disk surrounding the young Sun.

Author contributions: R.T., M.C., and F.R. designed research; R.T. performed research; R.T., M.C., A.G., and F.D. contributed new reagents/analytic tools; R.T. analyzed data; and R.T., M.C., A.G., F.D., and F.R. wrote the paper.

The authors declare no conflict of interest.

This article is a PNAS Direct Submission.

Published under the PNAS license.

Data deposition: Raw data from this manuscript have been deposited in the Mendeley Data repository (dx.doi.org/10.17632/hwwsdz8997.1).

¹To whom correspondence should be addressed. Email: romain.tartese@manchester.ac.uk.

This article contains supporting information online at www.pnas.org/lookup/suppl/doi:10.1073/pnas.1808101115/-DCSupplemental.

Published online August 6, 2018.

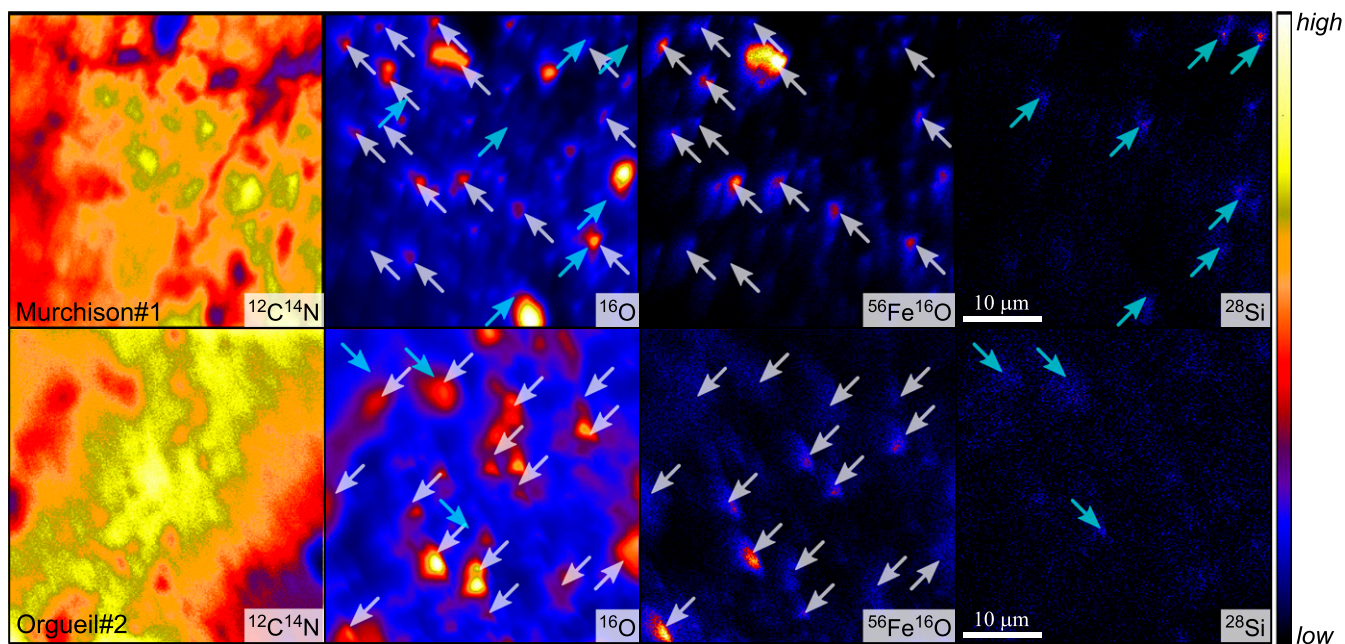


Fig. 2. NanoSIMS images showing the distribution of $^{12}\text{C}^{14}\text{N}$, ^{16}O , $^{56}\text{Fe}^{16}\text{O}$, and ^{28}Si secondary ion species in Murchison and Orgueil IOM acid maceration residues. White and cyan arrows indicate higher $^{56}\text{Fe}^{16}\text{O}$ and ^{28}Si intensities, respectively.

hypotheses over the other. Interestingly, $\delta^{18}\text{O}$ values obtained on CM chondrite bulk IOM are characterized by much larger variations (from -3.7% in Essebi to $+14.4\%$ in Murchison, both meteorites being observed falls) compared with other chondrite types (11, 12), which may either be related to variable contamination issues of bulk analyses or indicate that CM chondrites accreted IOM with variable O isotope compositions. Clearly, further bulk and in situ investigations are required to fully explore this issue.

Triple Oxygen Isotope Constraints on the Origin of Carbonaceous Chondrite IOM. The O isotope compositions estimated for Murchison IOM ($\delta^{17,18}\text{O} =$ approximately $+3\text{--}5\%$) and Orgueil IOM ($\delta^{17,18}\text{O} =$ approximately $+17\%$) fall on the slope 1 line in a $\delta^{17}\text{O}$ vs. $\delta^{18}\text{O}$ diagram (Fig. 5). As highlighted by Alexander

et al. (11), $\delta^{18}\text{O}$ values of the CI and CM chondrite IOM are similar to those of their matrix component (Fig. 5). However, the bulk and matrix $\delta^{17}\text{O}$ values obtained in CI chondrites appear to be lower compared with the $\delta^{17}\text{O}$ of Orgueil IOM (Fig. 5). These results, combined with the O isotope composition of CI–CM chondrite original anhydrous silicates, of matrix silicates, and of primordial alteration waters (which are thought to be similar for CI and CM chondrite parent bodies; refs. 21 and 26–29), thus seem to rule out scenarios in which the O isotope composition of O-bearing functional groups in CI chondrite IOM resulted from O isotope exchange between organic precursors and silicate components during aqueous alteration on the CI chondrite parent body (Fig. 5). On the other hand, because of the larger uncertainty associated with the $\delta^{17,18}\text{O}$ estimates for Murchison

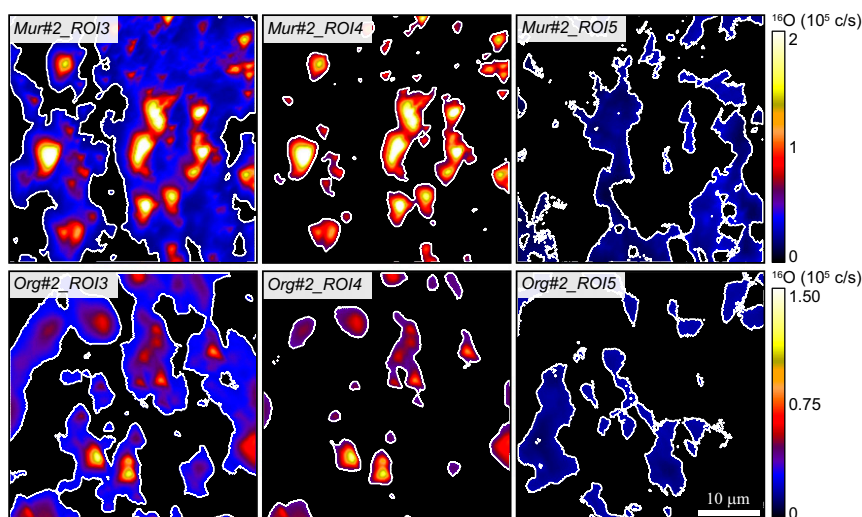


Fig. 3. Examples of the ROIs defined on ^{16}O ion images for one analysis each of Murchison and Orgueil acid residues. ROI#3 (Left) corresponds to intermediate O intensity, ROI#4 (Center) corresponds to O hot spots, and ROI#5 (Right) corresponds to pure IOM (see text for details).

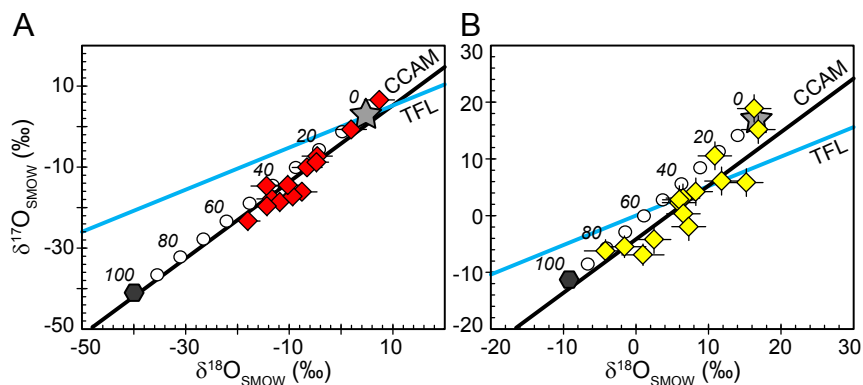


Fig. 4. Calculated O isotope values for mixed compositions between the estimated IOM $\delta^{17,18}\text{O}$ values (gray stars) in (A) Murchison and (B) Orgueil acid residues and the most negative $\delta^{17,18}\text{O}$ values measured in mineral phases in both Murchison (approximately -40‰ for spinel; ref. 21) and Orgueil (approximately -10‰ for olivine; ref. 22) (dark gray hexagons). White dots represent 10% mixing intervals, and 20% mixing intervals are given on the diagrams from 0 to 100% mineral contribution.

IOM, its formation during hydrothermal alteration on the CM parent body cannot be totally excluded.

The limited existing O isotope dataset obtained on a handful of CC meteorites so far suggests that IOM in the CI chondrite Orgueil tends to be enriched in $^{17,18}\text{O}$ compared with IOM in the CM chondrite Murchison (Fig. 5). Interestingly, this relationship is consistent with the variations of average H and N isotope compositions in CM and CI IOM, where CI IOM is enriched in D and ^{15}N compared with CM IOM (11, 12). The D and ^{15}N enrichments commonly observed in CC IOM have generally been attributed to low-temperature processes ($<150\text{ K}$) such as ion–molecule reactions taking place in dense interstellar media or at the surface of the PSN. However, recent experimental studies focused on the IOM molecular structure (9, 39), its bulk D/H (40) and the occurrence of D/H hot spots (41), and its noble gas isotope signatures (9), have argued that CC IOM could be produced by photochemical reactions involving organic radicals and taking place in the PSN regions where solar UV irradiation would have induced dissociation of C_xH_y molecules. Experiments have shown that photochemical reactions can produce mass-independent O isotope anomalies (e.g., refs. 42–44).

One could thus postulate that the mass-independent isotopic fractionation of oxygen isotopes in CC IOM also resulted from chemical reactions involving radical chemistry of CHON-bearing species in the PSN. If correct, such an effect now remains to be experimentally documented in a setting relevant to organics formation.

Cosmochemical Implications. The O isotope compositions estimated for CI–CM chondrite IOM fall on a slope 1 line in a $\delta^{17}\text{O}$ vs. $\delta^{18}\text{O}$ diagram, which, at a larger scale, describes the O isotope variations of most Solar System objects such as the Sun, high-temperature phases (i.e., CAI and chondrules) formed during the first few million years of Solar System evolution, and terrestrial planets for example (Fig. 5). However, the origin of this slope 1 line in planetary materials is still unknown. A possible mechanism involves self-shielding of ^{16}O -rich CO gas by UV light during photodissociation (e.g., ref. 42), but whether this occurred in the presolar molecular cloud (45) or in the PSN (46) remains debated. O isotope compositions of CC IOM appear to fall on a slope 1 line; it could thus be argued that oxygen contained in CC IOM derived from a combination of that found in

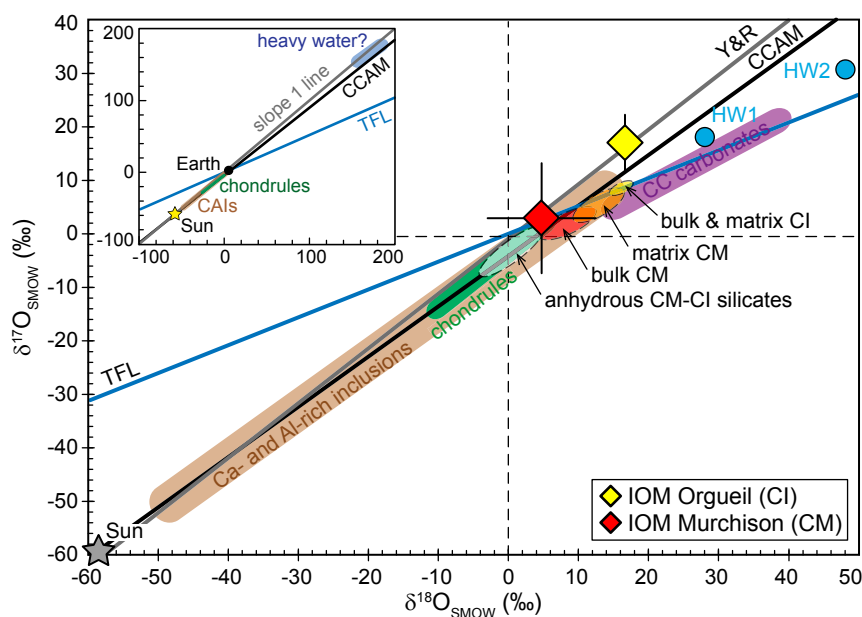


Fig. 5. O isotope compositions measured by L-SIMS on IOM residues isolated from the Orgueil and Murchison carbonaceous chondrites. The terrestrial fractionation line (TFL), the CCAM line, and the Y&R line are also represented, together with the O isotope compositions of the Sun (17), of CI and CM chondrite components (bulk, matrix, and anhydrous silicates; refs. 21, 22, 26, and 27), of carbonaceous chondrite Ca- and Al-rich inclusions (30–32), chondrules (33–37), and carbonates (38). Estimates for the O isotope composition of CM chondrite primordial water (HW1 and HW2) are from ref. 27 for HW1 and ref. 38 for HW2.

^{16}O -rich CO and $^{17,18}\text{O}$ -rich H_2O molecules formed as a result of self-shielding. If the different CC parent bodies accreted IOM sourced from a common carbonaceous reservoir, formed in the presolar molecular cloud, one may expect the various asteroidal parent bodies to have accreted presolar IOM grains characterized by similar O isotope compositions. The different triple O isotope compositions for Orgueil and Murchison IOM, dispersed along the slope 1 line, do not seem to favor such a scenario. Alternatively, and considering that Murchison and Orgueil IOM O isotope compositions are representative of those of CM and CI IOM in general, the observation that $\delta^{17,18}\text{O}_{\text{CM IOM}} < \delta^{17,18}\text{O}_{\text{CI IOM}}$, consistently with what has been measured for H and N isotope data ($\delta\text{D}_{\text{CM IOM}} < \delta\text{D}_{\text{CI IOM}}$ and $\delta^{15}\text{N}_{\text{CM IOM}} < \delta^{15}\text{N}_{\text{CI IOM}}$; refs. 11 and 12), may indicate that carbonaceous asteroids accreted IOM that formed locally in the PSN through photochemical radical chemistry involving CHON-bearing species (9, 41). Because of its elevated δD and $\delta^{15}\text{N}$ values, it has been proposed that CR IOM could represent the least processed IOM component accreted in carbonaceous asteroids (see discussion in ref. 2). Based on the observed relationship between H, N, and O isotope compositions in CI and CM chondrite IOM, we would expect CR chondrite IOM to have $\delta^{17,18}\text{O}$ values higher than those of CI chondrite IOM. Determining with high precision the triple O isotope composition of CR chondrite IOM would thus provide important constraints to further explore the formation mechanism(s) of CC IOM.

Materials and Methods

Organic Matter Isolation. IOM was isolated from the Orgueil, Murchison, and Cold Bokkeveld carbonaceous chondrite meteorites through successive demineralization using a HF/HCl acidic treatment (47). Powdered meteorite samples were first stirred at room temperature in water, followed by $\text{CH}_2\text{Cl}_2/\text{MeOH}$ [2/1 (vol/vol)], to remove soluble organic compounds. Carbonates were then removed at room temperature using 6 M HCl to minimize the formation of fluorides during HF/HCl maceration. Samples were then centrifuged and washed with distilled water until reaching neutrality. Isolation of IOM was achieved through acid maceration at room temperature in a HF/HCl mixture [2/1 (vol/vol)]. Samples were further centrifuged and washed with distilled water to reach neutrality. Neoformed fluorides were then degraded using 6 M HCl at 60 °C for 24 h. After HCl hot-acid maceration, IOM residues were washed with distilled water until reaching neutrality and thoroughly dried. For SIMS investigations, a few milligrams of IOM samples were pressed into high-purity indium (99.999%) and carbon coated.

IMS 1270/80 Secondary Ion Mass Spectrometry. Triple O isotope compositions of the IOM samples were measured using the CAMECA IMS 1270 E7 and 1280 HR2 ion probe instruments at the Centre de Recherches Pétrographiques et Géochimiques in Nancy, France, over several analytical sessions, using identical analytical protocols. Negative $^{16}\text{O}^-$, $^{17}\text{O}^-$, and $^{18}\text{O}^-$ secondary ions produced using a ~ 10 -nA Cs^+ primary beam, accelerated at 10 kV and rastered over ~ 20 - μm diameter areas, were measured in multicollection mode with one Faraday cup (FC) on the L'2 trolley for $^{16}\text{O}^-$ and two electron multipliers (EMs) for $^{17}\text{O}^-$ (central EM) and $^{18}\text{O}^-$ (H2 EM). To maximize peak flatness, entrance and exit slits were adjusted to achieve a mass resolving power of $\sim 8,000$ for $^{17}\text{O}^-$ on the central EM and $\sim 2,500$ on the off-axis L'2 FC and H2 EM (using slit #1 of the off-axis collectors). OM samples contain significant amounts of OH (average $^{16}\text{OH}^-/^{17}\text{O}^-$, $\sim 97 \pm 17$, $\sim 120 \pm 31$, and $\sim 121 \pm 20$ in Orgueil IOM, Murchison IOM, and Cold Bokkeveld IOM, respectively), and the protocol used did not completely eliminate contribution from the $^{16}\text{OH}^-$ tail on the $^{17}\text{O}^-$ peaks. To quantify this contribution and adequately correct the measured $^{17}\text{O}/^{16}\text{O}$ ratios, we assumed that the $^{16}\text{OH}^-$ peak was symmetrical, calculated the mass difference between the center of the $^{17}\text{O}^-$ (16.9991 amu) and $^{16}\text{OH}^-$ (17.0027 amu) peaks, and counted the $^{16}\text{OH}^-$ tail intensity at mass 17.0063 amu (mass $^{16}\text{OH}^- + [\text{mass } ^{16}\text{OH}^- - \text{mass } ^{17}\text{O}^-]$) for 50 s before and after each analysis. The $^{16}\text{OH}^-$ tail/peak ratios were $\sim 1.5 \pm 0.5 \times 10^{-5}$ in Murchison IOM, $\sim 1.1 \pm 0.1 \times 10^{-5}$ in Cold Bokkeveld, and $\sim 1.9 \pm 0.5 \times 10^{-5}$ in Orgueil IOM. This resulted in correction of the measured $\delta^{17}\text{O}$ values by 0.7–2.8‰ in Murchison IOM, 1.3–1.8‰ in Cold Bokkeveld IOM, and 0.8–2.4‰ in Orgueil IOM (SI Appendix, Table S1). For each analysis, the FC background was measured during presputtering. Dead time of the EMs was also calibrated once per analytical session. The total analysis time was 260 s (60-s presputtering and 40 cycles of 5 s each measurement time).

Instrumental mass fractionation (IMF) for O isotope measurements in IOM samples was corrected by repeated analyses of our Clarno kerogen standard ($\delta^{18}\text{O}_{\text{bulk}} = 14.3 \pm 0.1\text{‰}$; ref. 48), for which we assumed a $\delta^{17}\text{O}_{\text{bulk}}$ of 7.4‰, that is, a terrestrial O isotope composition. Count rates obtained on the Clarno kerogen standard were $0.3\text{--}1.2 \times 10^7$ cps-nA $^{-1}$ for $^{16}\text{O}^-$, $1.1\text{--}4.5 \times 10^3$ cps-nA $^{-1}$ for $^{17}\text{O}^-$ and $0.6\text{--}2.3 \times 10^4$ cps-nA $^{-1}$ for $^{18}\text{O}^-$, similar to those obtained on the IOM samples ($0.3\text{--}3.1 \times 10^7$ cps-nA $^{-1}$ for $^{16}\text{O}^-$, $0.1\text{--}1.1 \times 10^4$ cps-nA $^{-1}$ for $^{17}\text{O}^-$ and $0.5\text{--}5.5 \times 10^4$ cps-nA $^{-1}$ for $^{18}\text{O}^-$). The final uncertainties for individual $\delta^{17,18}\text{O}$ values, reported in SI Appendix, Table S1 at the 2σ level, include uncertainties related to counting statistics associated with each individual analysis and the external reproducibility measured for $\delta^{17,18}\text{O}$ values on the Clarno kerogen standard. Over three analytical sessions in February 2016, July 2016, and December 2016, we obtained a weighted average $\Delta^{17}\text{O}$ of $-0.1 \pm 0.4\text{‰}$ (95% confidence level, $n = 66$, mean square weighted deviation = 3.0) (SI Appendix, Fig. S1). We further tested our analytical protocol on the Silurian Zdanow terrestrial kerogen and obtained an average $\delta^{18}\text{O}_{\text{SIMS}}$ of $12.4 \pm 4.6\text{‰}$ (2 SD; $n = 9$), which is consistent with its bulk $\delta^{18}\text{O}$ of $13.4 \pm 0.2\text{‰}$ (48). The $\Delta^{17}\text{O}$ measured on Zdanow was $0.2 \pm 1.8\text{‰}$ (2 SD; $n = 9$), indicating that Zdanow sits on the terrestrial fractionation line (TFL), which shows that our L-SIMS protocol accurately measures the triple O isotope composition of organic residues.

The secondary species $^{12}\text{C}^{1}\text{H}$, ^{16}O , ^{28}Si , ^{32}S , and $^{56}\text{Fe}^{16}\text{O}$ were collected following O isotope analyses on the same analytical spots using the magnetic peak switching mode and a ~ 10 -nA Cs^+ beam to identify and filter the IOM data largely affected by contamination by residual silicate and oxide phases (see details in refs. 48 and 49).

Nanoscale Secondary Ion Mass Spectrometry. The triple O isotope composition of the Orgueil and Murchison IOM residues was also measured using the CAMECA NanoSIMS 50L ion probe instrument at The University of Manchester. Negative $^{16}\text{O}^-$, $^{17}\text{O}^-$, $^{18}\text{O}^-$, $^{12}\text{C}_2^-$, $^{12}\text{C}^{14}\text{N}^-$, $^{28}\text{Si}^-$, and $^{56}\text{Fe}^{16}\text{O}^-$ secondary ion species produced using a ~ 15 -pA Cs^+ primary beam, accelerated at 16 kV and rastered over $40 \mu\text{m} \times 40\text{-}\mu\text{m}$ areas, were measured in multicollection mode on seven EMs. Before analysis, a ~ 100 -pA Cs^+ primary beam was rastered over $50 \times 50\text{-}\mu\text{m}$ areas for 5 min to clean the sample surface and reach sputtering equilibrium. To limit the $^{16}\text{OH}^-$ interference on the $^{17}\text{O}^-$ peak, a $10\text{-}\mu\text{m}$ -wide entrance slit (E55) was used at the entrance of the mass analyzer, and a $150\text{-}\mu\text{m}$ -wide aperture slit (AS3) reduced the beam divergence, resulting in a mass resolving power of $\sim 8,000$. An electron gun was used for charge compensation. Using these conditions, the count rates were 15,000–35,000 cps for ^{16}O , 500–1,800 cps for $^{12}\text{C}_2$, 3,000–10,000 cps for $^{12}\text{C}^{14}\text{N}$, and 5–20 cps for $^{56}\text{Fe}^{16}\text{O}$, ensuring no detector aging over the week-long analytical session. During the session, the vacuum in the analysis chamber remained constant at $\sim 3 \times 10^{-10}$ mbar. For data acquisition, the $40\text{-}\mu\text{m}^2$ areas were divided in 256×256 pixels and between 320 and 600 frames were acquired at $1,000 \mu\text{s}/\text{px}$, resulting in a total analysis time of 6–11 h per analysis. Automatic alignment of the secondary beam (EOS, Cy, and P2/P3) and of the peak positions was performed every 50 frames during each analysis based on scanning the $^{16}\text{O}^-$ peak. IMF for O isotope measurements in IOM samples was corrected by analyzing the same Clarno kerogen standard used for the L-SIMS analyses (see above). The final uncertainties for individual $\delta^{17,18}\text{O}$ values, reported in SI Appendix, Table S2 at the 2σ level, include those related to counting statistics for each individual analysis and the external reproducibility measured for $\delta^{17,18}\text{O}$ on the Clarno kerogen standard ($\pm 11.1\text{‰}$ and $\pm 11.9\text{‰}$ for $\delta^{18}\text{O}$ and $\delta^{17}\text{O}$, respectively; 2 SE, $n = 3$).

The NanoSIMS data were processed off-line using the I'Image software package (L. Nittler, Carnegie Institution of Washington, Washington, DC). A 44-s dead time was applied to all EMs, and individual frames were binned into packages of 6–10 frames for each analysis to handle these large datasets more easily. ROIs were defined using lower and upper thresholds for the different species and comprised, for each analysis, the whole analyzed area, an area with intermediate ^{16}O intensity, and a ^{16}O -rich area corresponding to hot spots. A ROI of "pure IOM" was then defined by subtracting the ROI corresponding to the area with intermediate ^{16}O intensity to the ROI corresponding to the whole analyzed area. The $^{17}\text{O}/^{16}\text{O}$, $^{18}\text{O}/^{16}\text{O}$, $^{12}\text{C}^{14}\text{N}/^{12}\text{C}_2$, and $^{16}\text{O}/^{12}\text{C}_2$ ratios were calculated using I'Image.

All processed data are given in SI Appendix, Tables S1 and S2.

ACKNOWLEDGMENTS. We thank S. Derenne for providing the Murchison IOM sample, N. Bouden and J. Villeneuve for their help with L-SIMS analyses in Nancy, and I. C. Lyon for his help with NanoSIMS analyses in Manchester. We also thank the anonymous referees for their constructive reviews. This work was supported by European Research Council Grant PaleoNanoLife [290861; to principal investigator (PI) F.R.], Agence Nationale de la Recherche Grant CRADLE (ANR-15-CE31-0004-01; to PI M.C.), and UK Science and Technology Facilities Council Grants ST/M001253/1 (to

project co-investigator I. C. Lyon) and ST/P005225/1 (to PI R.T.). The NanoSIMS at The University of Manchester was funded by UK Research Partnership Investment Funding Manchester Research Partnership Investment

Funding Round 2. This is Institut de Physique du Globe de Paris Contribution 3964 and Centre de Recherches Pétrographiques et Géochimiques Contribution 2598.

- Hayes JM (1967) Organic constituents of meteorites—a review. *Geochim Cosmochim Acta* 31:1395–1440.
- Alexander CMO'D, Cody GD, De Gregorio BT, Nittler LR, Stroud RM (2017) The nature, origin and modification of insoluble organic matter in chondrites, the major source of Earth's C and N. *Chem Erde Geochem* 77:227–256.
- Robert F, Epstein S (1982) The concentration and isotopic composition of hydrogen, carbon and nitrogen in carbonaceous meteorites. *Geochim Cosmochim Acta* 46: 81–95.
- Yang J, Epstein S (1983) Interstellar organic matter in meteorites. *Geochim Cosmochim Acta* 47:2199–2216.
- Busemann H, et al. (2006) Interstellar chemistry recorded in organic matter from primitive meteorites. *Science* 312:727–730.
- Remusat L, Palhol F, Robert F, Derenne S, France-Lanord C (2006) Enrichment of deuterium in insoluble organic matter from primitive meteorites: A solar system origin? *Earth Planet Sci Lett* 243:15–25.
- Gourier D, et al. (2008) Extreme deuterium enrichment of organic radicals in the Orgueil meteorite: Revisiting the interstellar interpretation? *Geochim Cosmochim Acta* 72:1914–1923.
- Derenne S, Robert F (2010) Model of molecular structure of the insoluble organic matter isolated from Murchison meteorite. *Meteorit Planet Sci* 45:1461–1475.
- Kuga M, Marty B, Marrocchi Y, Tissandier L (2015) Synthesis of refractory organic matter in the ionized gas phase of the solar nebula. *Proc Natl Acad Sci USA* 112: 7129–7134.
- Cody GD, et al. (2011) Establishing a molecular relationship between chondritic and cometary organic solids. *Proc Natl Acad Sci USA* 108:19171–19176.
- Alexander CMO'D, Fogel M, Yabuta H, Cody GD (2007) The origin and evolution of chondrites recorded in the elemental and isotopic compositions of their macromolecular organic matter. *Geochim Cosmochim Acta* 71:4380–4403.
- Alexander CMO'D, et al. (2010) Deuterium enrichments in chondritic macromolecular material—implications for the origin and evolution of organics, water and asteroids. *Geochim Cosmochim Acta* 74:4417–4437.
- Orthous-Daunay FR, et al. (2013) Mid-infrared study of the molecular structure variability of insoluble organic matter from primitive chondrites. *Icarus* 223:534–543.
- Quirico E, et al. (2014) Origin of insoluble organic matter in type 1 and 2 chondrites: New clues, new questions. *Geochim Cosmochim Acta* 136:80–99.
- Hashiguchi M, Kobayashi S, Yurimoto H (2015) Deuterium- and ¹⁵N-signatures of organic globules in Murchison and Northwest Africa 801 meteorites. *Geochem J* 49: 377–391.
- Clayton RN (1993) Oxygen isotopes in meteorites. *Annu Rev Earth Planet Sci* 21: 115–149.
- McKeegan KD, et al. (2011) The oxygen isotopic composition of the Sun inferred from captured solar wind. *Science* 332:1528–1532.
- Le Guillou C, Bernard S, Brearley AJ, Remusat L (2014) Evolution of organic matter in Orgueil, Murchison and Renazzo during parent body aqueous alteration: In situ investigations. *Geochim Cosmochim Acta* 131:368–392.
- Clayton RN, Onuma N, Grossman L, Mayeda TK (1977) Distribution of the presolar component in Allende and other carbonaceous chondrites. *Earth Planet Sci Lett* 34: 209–224.
- Young ED, Russell SS (1998) Oxygen reservoirs in the early solar nebula inferred from an Allende CAI. *Science* 282:452–455.
- Clayton RN, Mayeda TK (1984) The oxygen isotope record in Murchison and other carbonaceous chondrites. *Earth Planet Sci Lett* 67:151–161.
- Leshin LA, Rubin AE, McKeegan KD (1997) The oxygen isotopic composition of olivine and pyroxene from CI chondrites. *Geochim Cosmochim Acta* 61:835–845.
- Halbout J, Robert F, Javoy M (1990) Hydrogen and oxygen isotope compositions in kerogen from the Orgueil meteorite: Clues to a solar origin. *Geochim Cosmochim Acta* 54:1453–1462.
- Kroopnick P, Craig H (1972) Atmospheric oxygen: Isotopic composition and solubility fractionation. *Science* 175:54–55.
- Luz B, Barkan E (2011) The isotopic composition of atmospheric oxygen. *Global Biogeochem Cycles* 25:GB3001.
- Rowe MW, Clayton RN, Mayeda TK (1994) Oxygen isotopes in separated components of CI and CM meteorites. *Geochim Cosmochim Acta* 58:5341–5347.
- Clayton RN, Mayeda TK (1999) Oxygen isotope studies of carbonaceous chondrites. *Geochim Cosmochim Acta* 63:2089–2104.
- Fujiya W (2018) Oxygen isotopic ratios of primordial water in carbonaceous chondrites. *Earth Planet Sci Lett* 481:264–272.
- Marrocchi Y, Bekaert DV, Piani L (2018) Origin and abundance of water in carbonaceous asteroids. *Earth Planet Sci Lett* 482:23–32.
- Aléon J, El Goresy A, Zinner E (2007) Oxygen isotope heterogeneities in the earliest protosolar gas recorded in a meteoritic calcium–aluminum-rich inclusion. *Earth Planet Sci Lett* 263:114–127.
- Krot AN, et al. (2008) Oxygen isotopic compositions of Allende type C CAIs: Evidence for isotopic exchange during nebular melting and asteroidal metamorphism. *Geochim Cosmochim Acta* 72:2534–2555.
- Bodénan JD, Starkey NA, Russell SS, Wright IP, Franchi IA (2014) An oxygen isotope study of Wark-Lovering rims on type A CAIs in primitive carbonaceous chondrites. *Earth Planet Sci Lett* 401:327–336.
- Clayton RN, et al. (1983) Oxygen isotopic compositions of chondrules in Allende and ordinary chondrites. *Chondrules and Their Origins*, ed King EA (Lunar and Planetary Institute, Houston), pp 37–43.
- Rubin AE, Wasson JT, Clayton RN, Mayeda TK (1990) Oxygen isotopes in chondrules and coarse-grained chondrule rims from the Allende meteorite. *Earth Planet Sci Lett* 96:247–255.
- Weisberg MK, Prinz M, Clayton RN, Mayeda TK (1993) The CR (Renazzo-type) carbonaceous chondrite group and its implications. *Geochim Cosmochim Acta* 57: 1567–1586.
- Jones RH, et al. (2004) Oxygen isotope heterogeneity in chondrules from the Mokoia CV3 carbonaceous chondrite. *Geochim Cosmochim Acta* 68:3423–3438.
- Jenniskens P, et al.; Sutter's Mill Meteorite Consortium (2012) Radar-enabled recovery of the Sutter's Mill meteorite, a carbonaceous chondrite regolith breccia. *Science* 338: 1583–1587.
- Verdier-Paoletti MJ, et al. (2017) Oxygen isotope constraints on the alteration temperatures of CM chondrites. *Earth Planet Sci Lett* 458:273–281.
- Biron K, Derenne S, Robert F, Rouzaud JN (2015) Toward an experimental synthesis of the chondritic insoluble organic matter. *Meteorit Planet Sci* 50:1408–1422.
- Laurent B, et al. (2015) The deuterium/hydrogen distribution in chondritic organic matter attests to early ionizing irradiation. *Nat Commun* 6:8567.
- Robert F, et al. (2017) Hydrogen isotope fractionation in methane plasma. *Proc Natl Acad Sci USA* 114:870–874.
- Thiemens MH, Heidenreich JE, 3rd (1983) The mass-independent fractionation of oxygen: A novel isotope effect and its possible cosmochemical implications. *Science* 219:1073–1075.
- Chakraborty S, Ahmed M, Jackson TL, Thiemens MH (2008) Experimental test of self-shielding in vacuum ultraviolet photodissociation of CO. *Science* 321:1328–1331.
- Chakraborty S, Yanchulova P, Thiemens MH (2013) Mass-independent oxygen isotopic partitioning during gas-phase SiO₂ formation. *Science* 342:463–466.
- Yurimoto H, Kuramoto K (2004) Molecular cloud origin for the oxygen isotope heterogeneity in the solar system. *Science* 305:1763–1766.
- Lyons JR, Young ED (2005) CO self-shielding as the origin of oxygen isotope anomalies in the early solar nebula. *Nature* 435:317–320.
- Durand B, Nicaise G (1980) Procedures for kerogen isolation. *Kerogen: Insoluble Organic Matter from Sedimentary Rocks*, ed Durand B (Technip, Paris), pp 35–54.
- Tartèse R, Chaussidon M, Gurenko A, Delarue F, Robert F (2016) In situ oxygen isotope analysis of fossil organic matter. *Geochim Cosmochim Acta* 182:24–39.
- Tartèse R, Chaussidon M, Gurenko A, Delarue F, Robert F (2017) Warm Archaean oceans reconstructed from oxygen isotope composition of early-life remnants. *Geochem Perspect Lett* 3:55–65.